Detection limits for close eclipsing and transiting sub-stellar and planetary companions to white dwarfs in the WASP survey

F. Faedi,[1,2][*] R. G. West,[1] M. R. Burleigh,[1] M. R. Goad,[1] L. Hebb,[3,4]

[1] *Department of Physics and Astronomy, University of Leicester, University Road, Leicester, LE1 7RH, U.K.*
[2] *Astrophysics Research Centre, School of Mathematics and Physics, Queens University, University Road, Belfast, BT7 1NN, U.K.*
[3] *School of Physics and Astronomy, University of St. Andrews, North Haugh, Fife, KY16 9SS, U.K.*
[4] *Department of Physics and Astronomy, Vanderbilt University, Nashville, TN 37235, U.S.A.*

ABSTRACT
We have performed extensive simulations to explore the possibility of detecting eclipses and transits of close, sub-stellar and planetary companions to white dwarfs in WASP light curves. Our simulations cover companions $\sim 0.3\,R_\oplus < R_{pl} < 12\,R_\oplus$ and orbital periods $2h < P < 15d$, equivalent to orbital radii $0.003AU < a < 0.1AU$. For Gaussian random noise WASP is sensitive to transits by companions as small as the Moon orbiting a V $\simeq 12$ white dwarf. For fainter white dwarfs WASP is sensitive to increasingly larger radius bodies. However, in the presence of correlated noise structure in the light curves the sensitivity drops, although Earth-sized companions remain detectable in principle even in low S/N data. Mars-sized, and even Mercury-sized bodies yield reasonable detection rates in high-quality light curves with little residual noise. We searched for eclipses and transit signals in long-term light curves of a sample of 194 white dwarfs resulting from a cross-correlation of the McCook & Sion catalogue and the WASP archive. No evidence for eclipsing or transiting sub-stellar and planetary companions was found. We used this non-detection and results from our simulations to place tentative upper limits to the frequency of such objects in close orbits at white dwarfs. While only weak limits can be placed on the likely frequency of Earth-sized or smaller companions, brown dwarfs and gas giants (radius $\approx R_{jup}$) with periods $< 0.1 - 0.2$ days must certainly be rare ($< 10\%$). More stringent constraints likely requires significantly larger white dwarf samples, higher observing cadence and continuous coverage. The short duration of eclipses and transits of white dwarfs compared to the cadence of WASP observations appears to be one of the main factors limiting the detection rate in a survey optimised for planetary transits of main sequence stars.

Key words: method: data analysis - occultations - stars: planetary systems - stars: white dwarfs

1 INTRODUCTION

In recent years we have witnessed considerable progress in the search for extra-solar planets. Since the first detection of a 'Hot Jupiter' around the main-sequence star 51 Peg (Mayor & Queloz 1995), the number of extra-solar planets has rapidly risen, and currently approaching 500. Most of these discoveries are the result of radial velocity (RV) searches. More recently, an increasing number of extra-solar planets (> 80) have been detected by dedicated planetary transit surveys including HATnet (Bakos et al. 2004), TrES

(e.g. Brown & Charbonneau 2000; Dunham et al. 2004; Alonso et al. 2004), OGLE (Udalski et al. 2002, 2003), XO (McCullough et al. 2005), and WASP, the UK Wide-Angle Search for Planets (Pollacco et al. 2006).

Planet detection via the transit technique involves searching for periodic dips in stellar light curves as a planet occludes a small fraction of the visible disc of the host star once per orbit. Only planets with their orbital planes aligned within a few degrees to the line of sight will exhibit a transit, the probability of such an alignment being around 10% for typical 'hot Jupiter' systems. This introduces a constraint on the number of observable systems and explains the relatively low number of transiting planets when compared to

* E-mail:f.faedi@qub.ac.uk

radial velocity studies. Importantly, when combined with RV measurements, planetary transits offer the unique possibility of deriving both the planet mass and radius, since for these systems the inclination i is well-known (Sackett 1999). For a given planetary radius, the transit depth is directly proportional to $(R_p/R_*)^2$, where R_p, and R_* are the planetary and stellar radii respectively. Therefore, planets orbiting solar-type stars have extremely shallow eclipses, blocking $\sim 1\%$ of the light for a giant planet and $\sim 0.01\%$ of the light for an Earth-sized planet. Current ground-based wide-field surveys can achieve the necessary photometric accuracy of better than 1%, only for the brightest stars (V ~ 9–12 in the case of WASP), so the bulk of the planets discovered by transit surveys around main-sequence stars have radii in the range $R_p \sim 0.9$–$1.8\,R_{jup}$. To date the smallest extra-solar planet detected in a ground-based transit survey is HAT-P-11b, a Neptune-size planet ($R_p = 0.452\,R_{jup}$) transiting a K dwarf star (Bakos et al. 2010).

A major advantage over main sequence primaries is offered by white dwarf stars. White dwarfs (WDs) are compact degenerate objects with $R_{WD} \sim 1\,R_\oplus$ (Earth radius), and represent the final stage of evolution of main$-$sequence stars with masses $\leqslant 8\,M_\odot$ (i.e. $\sim 97\%$ of all stars in our galaxy). Any sub-stellar or gas giant companion orbiting the star, will completely eclipse it, while bodies as small as the Moon will display relatively large transit depths ($\sim 3\%$), with the only caveat being that it remains unclear as to whether any such systems survive beyond the latter stages of stellar evolution. The strong gain in the planet$-$to$-$star relative dimensions opens up the possibility of detecting low$-$mass sub$-$stellar and in particular terrestrial objects in orbit around WDs. In Sections 1.1, 1.2 we briefly discuss theoretical studies concerned with the likelihood of sub-stellar and planetary survival to stellar evolution.

1.1   Sub-stellar companions to WDs

Observationally, sub-stellar companions to WDs are found to be rare. Using the 2MASS survey, Farihi et al. (2005) estimated that $< 0.5\%$ of WDs have L dwarf companions. More recently, excess near-infrared emission from WDs in the UKIDSS survey (Steele et al. in preparation) tentatively suggests the fraction of unresolved brown dwarf companions (including T dwarfs) may be slightly higher, between $1-2\%$. However, at the time of writing only three wide WD+BD systems have been spectroscopically confirmed, GD 165 (Becklin & Zuckerman 1988), PHL5038 (Steele et al. 2009), and LSPM 1459 + 0857 AB (Day-Jones et al. 2010) and two detached, non-eclipsing, short-period WD+BD systems are currently known, WD0137 $- 349$ (Maxted et al. 2006, Burleigh et al. 2006, $P \approx 116$m), and GD1400 (Farihi & Christopher 2004, Dobbie et al. 2005, Burleigh et al., in preparation, $P \approx 9.9$h). GD1400B and WD0137 $-$ 349B are the only two sub-stellar companions known to have survived the common envelope (CE) phase of stellar evolution, with WD0137 $- 349$B currently the lowest mass ($\sim 50\,M_{jup}$) object known to have done so.

Although infrared sky surveys such as UKIDSS, VISTA and WISE, and observatories such as Spitzer hope to reveal many more such binaries, they remain difficult to identify either as infra-red excesses or through radial velocity measurements. The detection of more close systems will allow us to place observational upper limits on the mass of sub-stellar companions that can survive CE evolution. Furthermore, examples of eclipsing WD+BD binaries will be important for exploring the WD and substellar mass-radius relations (e.g. Parsons et al. 2010).

In addition the detection of a significant number of eclipsing WD+BD binary systems might help uncover the hypothesised population of 'old' cataclysmic variables (CVs) in which the current accretion rate is extremely low and the companion has been reduced to substellar mass (e.g. Patterson 1998; Patterson et al. 2005; Littlefair et al. 2003). While these systems elude direct detection as X-ray sources and remain difficult to identify in optical and infra-red surveys, it is possible to measure the mass and the radius of the donor in eclipsing CVs. Littlefair et al. (2006) confirmed the first such system through eclipse measurements, while Littlefair et al. (2007) showed that another eclipsing CV, SDSS J150722.30 + 523039.8, was formed directly from a detached WD/BD binary. Old CVs are important for shedding light on models of close binary evolution as well as for placing constraints on the period distribution of cataclysmic variables; in particular, the period gap and the period minimum (King 1988; Parthasarathy et al. 2007).

1.2   Can planets survive stellar evolution?

Every star less massive than $8\,M_\odot$ ($\sim 97\%$ of all stars in our galaxy) will end its life as a WD. Thus, it is natural to ask what will be the fate of known extra-solar planetary systems? This question also has particular interest for us, in that the Earth's survival to the Sun's post-main sequence evolution is uncertain (Rasio et al. 1996; Duncan & Lissauer 1998; Villaver & Livio 2007). Several theoretical studies discuss post-main sequence evolution of planetary systems and show that planetary survival is not beyond possibility (Duncan & Lissauer 1998; Debes & Sigurdsson 2002; Burleigh et al. 2002; and Villaver & Livio 2007). Radial velocity observations of red giants indicate that planets orbits beyond the radius of the star's envelope can survive stellar evolution to that stage (see Frink et al. 2002; Hatzes et al. 2005, Sato et al. 2003). However, direct imaging searches at WDs have so far failed to detect any planetary mass companions (e.g. Hogan et al. 2009). More recently, Silvotti et al. (2007) reported the detection of a $\sim 3\,M_{jup}$ planet orbiting an extreme horizontal branch star. Furthermore, Mullally et al. (2008) found convincing evidence of a $2\,M_{jup}$ planet in a 4.5 year orbit around a pulsating WD. The latter, if confirmed, will be the first planet detected in orbit around a WD, and will show that planets can indeed survive the death of their parent star.

The existence of short-period planetary companions to WDs may seem less likely. Two scenarios may give rise to planets in short-period orbits around WDs:
1) planets undergo CE evolution and survive their parent stars' evolution to a WD, or 2) their orbits are significantly changed by a process occurring at the end of the asymptotic giant branch (AGB) phase of stellar evolution.

Villaver & Livio (2007) investigated the fate of a planet engulfed by the envelope of an AGB star and suggested that planets in orbit within the reach of the AGB envelope will either totally evaporate or in rare cases, a more massive body may accrete mass and become a close companion to the star.

In this scenario only the massive companions (e.g. brown dwarfs like GD1400 and WD0137 − 349B) are likely to survive the red giant and the AGB phases of stellar evolution. However, estimates of the minimum substellar mass necessary for survival are highly uncertain and depend on several factors, for example, the efficiency of the envelope ejection (Villaver & Livio 2007 and references therein). None the less, it is unlikely that terrestrial planets can survive engulfment and evaporation (Wickramasinghe et al. 2010).

Planets that escape engulfment by the red giant or asymptotic giant and that are sufficiently far from the stellar surface that they do not experience tidal drag, will have their orbital radii increased to conserve angular momentum (as described by Jeans 1924). Duncan & Lissauer (1998) investigated the stability of planetary systems during post main-sequence evolution, and found that for WD progenitors experiencing substantial mass loss during the AGB phase, planetary orbits become unstable on timescales of $\leqslant 10^8$ year. Debes & Sigurdsson (2002) also studied the stability of planetary systems and found that mass loss from the central star is sufficient to destabilise planetary systems comprising two or more planets. For unstable systems in which the orbits happen to cross, Debes & Sigurdsson (2002) found that the most likely result was that one planet would be scattered into an inner orbit, while the other would either be boosted into a larger orbit, or ejected from the system altogether. This may result in WD systems which have settled into a configuration wherein planets are found at orbital radii which were originally occupied by the (now evaporated) inner planets before the RGB phase of stellar evolution.

The above scenario provides a plausible explanation for the recent detection of silicate-rich dust discs around a growing number of WDs at orbital radii up to $\sim 1\,R_\odot$ (e.g. Jura 2003; Reach et al. 2005; Farihi et al. 2008; Farihi et al. 2009).Jura (2003) suggests that the formation of dust discs around WDs is most probably due to the tidal disruption of an asteroid or larger body which has strayed too close to the parent star. Dynamical instabilities during the final stages of solar system evolution could have caused the rocky body to migrate inwards (as suggested by Debes & Sigurdsson 2002). If the body wanders too close to the Roche radius of the WD it will be completely destroyed, producing a debris disc reminiscent of Saturn's rings (Jura 2003). Recent studies of the dust disc around the WD GD 362 (Jura et al. 2009) suggest that the more likely scenario which simultaneously explains all of GD 362's distinctive properties is that we are witnessing the consequences of the tidal destruction of a single body that was as massive as Callisto or Mars.

Consideration of dynamical interactions and orbital stability indicates that while a terrestrial body may be perturbed from some wide orbit into an eccentric orbit that takes it within the Roche radius of a WD and hence be disrupted, it is highly unlikely for such an object to be captured into a stable, close orbit just beyond the Roche radius. None the less, one may speculate on the existence of 'shepherd moons' accompanying the dust discs detected at WDs, similar to those at Saturn's rings. Alternatively, when close, double WDs are drawn together by gravitational radiation and merge, second generation terrestrial planets may form in remnant discs left by the tidal disruption of the lower mass degenerate (Hansen 2002, Livio et al. 2005). Indeed,

Wickramasinghe et al. (2010) speculates that such an object may be closely orbiting the unusual magnetic WD GD 356. Thus, the existence of asteroids, moons and rocky planets in close orbits to WDs may not be entirely unreasonable.

The detection of short-period substellar and planetary-mass companions to WDs, will open an exciting chapter in the study of extra-solar planet evolution, constraining theoretical models of common envelope evolution and helping us to understand the ultimate fate of hot Jupiter systems as well as the fate of our own solar system in the post main-sequence phase. In this work we present the results of a study designed to investigate the detection limits for transiting sub−stellar and terrestrial companions in close orbits around WDs [1]. In Section 2 we describe briefly the WASP project and WASP telescopes, which provide the WD light curves which form the basis of our transit search. In Section 3 we outline our Monte Carlo simulations, describing our detection method, as well as characterising the type of systems we might hope to detect. In Section 4 we discuss the results of our simulations and provide transit recovery rates for simulated light curves comprising random Gaussian noise (white noise) and correlated noise (red noise). In Section 5 we present the results of a comprehensive transit search in a sample of 194 WD light curves found in the WASP archive. Finally, our conclusions are presented in Section 6.

2   THE WASP PROJECT

The WASP (Wide-Angle Search for Planets) project, operates two robotic telescopes, one located amongst the Isaac Newton Group of telescopes (ING), in La Palma Spain, with a second instrument situated at the South African Astronomical Observatory (SAAO). Each instrument consists of eight f/1.8 Canon lenses each with an Andor CCD array of 2048^2 13.5μm pixels, giving a field of view of 7.8 degrees square for each camera. The observation strategy is to cyclically raster the sky in a series of fields centred on the current local sidereal time and separated by 1 hour in right ascension. Each observation lasts for about 1 minute (30 seconds exposure, plus slew and telescope settling time). This strategy yields well sampled light curves with a typical cadence of about 8 minutes per field. WASP provides good quality photometry with accuracy $\leqslant 1\%$ in the magnitude range V $\sim$ 9–12. The WASP telescopes and data analysis strategies are described in detail in Pollacco et al. (2006).

3   DETECTABILITY OF ECLIPSES AND TRANSITS OF WHITE DWARFS

To assess the chances of detecting eclipses and transits of white dwarf host stars in ground-based wide-field surveys we performed an extensive set of Monte Carlo simulations. The approach we adopted was to create realistic synthetic light curves containing eclipse and transit signatures of the expected depth and duration for a range of companion size

---

[1] We note that Di Stefano et al. (2010) discuss the possibility of discovering asteroids and moons in much wider orbits around WDs in Kepler data.

and orbital period, then to attempt to detect these signatures using a standard transit-detection algorithm (box-least-squares, BLS). By noting the rate at which the BLS search recovered the transit at the correct period (or an integer multiple or fraction) we were able to estimate the feasibility of detecting such systems in an automated manner.

3.1   Characteristics of the transit signal

The probability ($p_{\rm tr}$) that a low mass star, brown dwarf or planet in a circular orbit will transit or eclipse its host star is given by

$$p_{\rm tr} \simeq \left(\frac{4\pi^2}{GM_*} \right)^{\frac{1}{3}} \frac{R_p + R_*}{P^{2/3}} \tag{1}$$

Assuming an orbital inclination $i = 90°$ the depth ($\delta_{\rm tr}$) and duration ($D_{\rm tr}$) of such a transit are given by

$$\delta_{\rm tr} = \frac{\Delta F}{F} = \begin{cases} R_p^2/R_*^2, & \text{for } R_p \leqslant R_* \\ 1, & \text{for } R_p > R_* \end{cases} \tag{2}$$

$$D_{\rm tr} = 2\sqrt{\frac{a}{GM_*}}(R_p + R_*) \tag{3}$$

For our simulations we have chosen the parameters of the host star to represent a typical 1-Gyr-old carbon-core WD of mass $M_* = 0.6\,{\rm M_\odot}$ and radius $R_* = 0.013\,{\rm R_\odot}$. We explored the detectability of planetary transits across the two-dimensional parameter space defined by the orbital period and the planet radius. We considered orbital periods in the range $P \sim 2$ hours to 15 days (equivalent to orbital distances of between $a \sim 0.003$ and 0.1 AU). The lower-limit to the orbital period was chosen to yield an orbital separation close to the Roche radius of the WD, the upper-limit by a requirement that we have a reasonable chance of detecting five or more transits in a typical 150 day observing season of a WASP survey field.

Figure 1 shows the probability that a given system will transit, and the depth and duration of such transits across this parameter space. It is evident from this diagram that the signatures of transits of WDs by typical planet-sized bodies will be rather different than those seen for typical transiting hot Jupiters. In particular the transit duration is much shorter for WDs than for normal stars (from $\sim$ 1–30 min for companions with sizes ranging from Moon-size to Jupiter-size, compared to 2–3 hours for a typical hot Jupiter), and the transit depths are much larger (from around 3% for a Moon-sized to 100% for any companion larger than the Earth, compared to $\sim$ 1% for a hot Jupiter).

3.2   Generation of synthetic light curves

The synthetic light curves were generated using the time sampling of a typical WASP survey field. light curves were generated with statistical signal-to-noise ratios representative of three magnitude ranges (V $\simeq$ 12, 13 and 15) spanning the range of brightness of WDs in the WASP survey. The corresponding photometric accuracy of WASP over this range is $\sim$1% to 10%. Because WASP data show residual covariant-noise structure due to instrumental systematics we have tested the transit recovery rate in the case
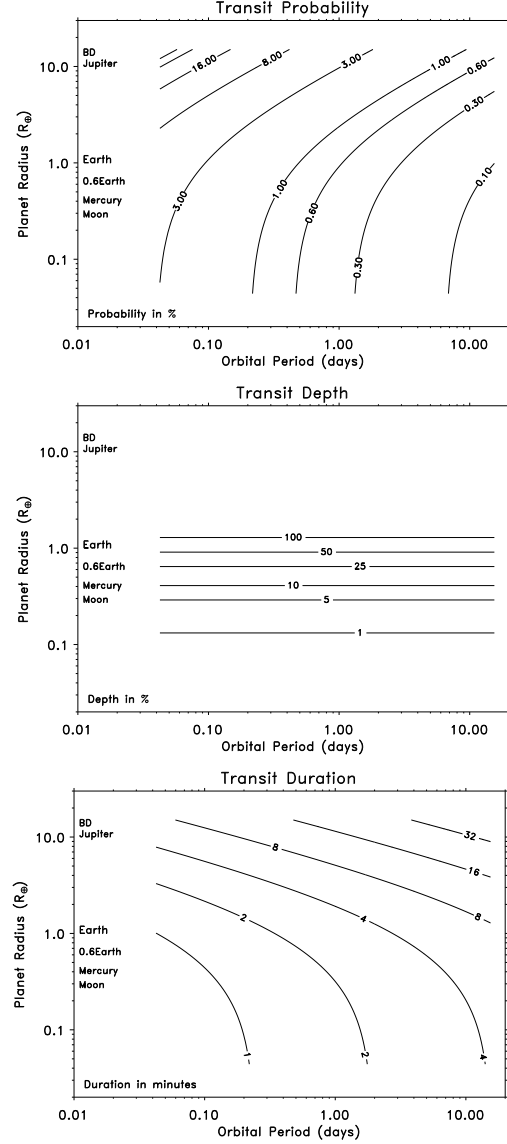

Figure 1. Contours of constant transit probability (top), depth (centre) and duration (bottom) in the parameter space defined by orbital period and planetary radius. The transit probability and depth are expressed in percentage values. The transit duration is expressed in minutes.

of both uncorrelated "white" noise and correlated "red" noise. In the white-noise case we injected transit-like signatures into otherwise non-variable light curves, adding a Gaussian-distributed noise component of standard deviation σ. We chose σ to be representative of the mean photometric error on the points obtained from a real WASP light curve for an object of our chosen magnitude. The template WASP light curves therefore defined the time-sampling and the average signal-to-noise, but the photometry was otherwise entirely synthetic. In the red noise case we injected fake transits into a set of unmodified WASP light curves obtained from a densely sampled field observed during the 2004 season. Data from the 2004 season have been detrended and thoroughly searched for transit-like events as described in Collier Cameron et al. (2006). Moreover,
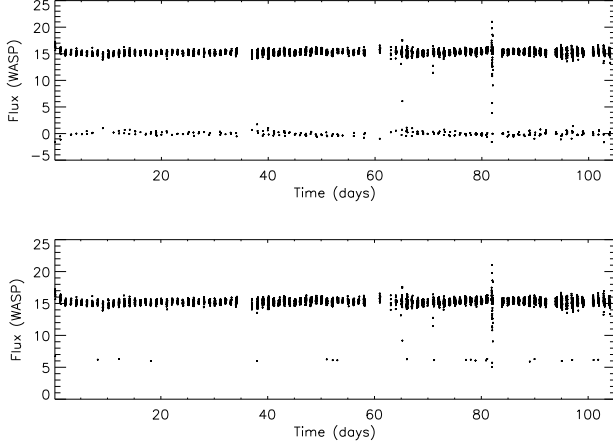
Figure 2. Two example synthetic light curves. Top, an eclipsing brown dwarf in an orbit with a period of 2 hr, around a WD. Bottom, a $1.2\,R_\oplus$ companion to a WD in 5 hr orbit.

we cross-correlated stars in the WASP field with the publicly available General Catalogue of Variable Stars (GCVS; Samus et al. 2004), and we evaluated the RMS of each light curve which we used to identify and remove variable objects after individual eye-balling. Finally, each light curve contained around 4240 data points, acquired over 116 nights, and spread across a baseline of 128 nights, with photometric accuracy raging from $\sim 1\%$ to $\sim 10\%$ for stars in the magnitude range $12 < V < 15$. For each light curve we used the WASP pipeline fluxes and errors derived after detrending by the SysRem algorithm (Collier Cameron et al. 2006).

Planet transit light curves of main-sequence stars show a characteristic shape, with an ingress lasting several tens of minutes, a flat bottom of 2–3 hours and an egress again lasting tens of minutes. For the case of a WD host star considered here, the ingress and egress duration is typically short compared to cadence of the WASP survey (8–10 minutes). We therefore ignore the detailed shape of the ingress and egress phases and modelled the transit signatures as simple box-like profiles.

To cover the orbital period-planet radius parameter space we selected seven trial periods spaced approximately logarithmically ($P = 0.08, 0.22, 0.87, 1.56, 3.57, 8.30$ and 14.72 days), and five planet radii $R_{\rm p} = 10.0, 1.0, 0.6, 0.34$ and $0.27\,R_\oplus$. We modelled the set of synthetic light curves by injecting fake transit signals into phase-folded light curves at the trial period with a random transit epoch t_0 in the range $0 < t_0 < P$. We computed the transit duration according to Equation 3, and hence the width of the transit in orbital phase $\phi_{\rm tr} = D_{\rm tr}/P$. For all data points falling in the phase range $0 \leqslant \phi_i \leqslant \phi_{\rm tr}$ we then reduced the observed flux by a factor $\delta_{\rm tr}$. For each combination of orbital period and planet radius we generated 100 synthetic light curves.

Figure 2 shows two examples of our simulated transit light curves. The top panel shows the synthetic light curve of an hypothetical eclipsing WD+BD binary system with an orbital period of $P = 116$ mins, similar to WD0137$-$349 (a non-eclipsing system, Maxted et al. 2006). The lower

panel shows the simulated transit light curve for a rocky body of radius $1.2\,R_\oplus$ in a 5 hr orbit.

3.3 Detection algorithm

To recover the transit signals from the synthetic light curves we used an implementation of the box-least-squares (BLS) algorithm (Kovács et al. 2002) commonly used to detect transits of main sequence stars. The BLS algorithm is most sensitive when the modelled box-width closely matches the duration of the true transit signal. Thus, to ensure that the BLS search was sensitive across the expected range of transit durations, we chose to search a grid of box widths $W_{\rm b} = \{1, 2, 4, 8, 16, 32\}$ minutes, covering the range in transit durations over most of our parameter space (Figure 1). We defined the grid of trial periods sampled by BLS as follows:

$$F_{\max} = \frac{1}{P_{\min}}, \qquad F_{\min} = \frac{1}{P_{\max}} \qquad (4)$$

where $P_{\min} = 2$ hr and $P_{\max} = 15$ day. The frequency interval was chosen such that the accumulated phase difference between successive trial frequencies over the duration of the light curve corresponds to the width of the shortest trial box duration at the longest period searched. At each trial frequency we defined a set of trial transit epochs at an interval $W_{\rm b}'$ chosen such that $W_{\rm b}' \simeq W_{\rm b}$ for the shortest trial box duration, adjusted to meet a constraint that the number of epochs $N_e = P/W_{\rm b}'$ be an integer.

Adopting the notation of Collier Cameron et al. (2006) we denote the set of observations in the light curve $\tilde{x}_i$ with formal variances σ_i^2 and additional variances $\sigma_{t(i)}^2$ computed by SysRem to account for transient systematic variations due to patchy atmospheric extinction, for example. For each data point we compute a weight

$$w_i = \frac{1}{\sigma_i^2 + \sigma_{t(i)}^2}$$

then subtract the weighted mean of the observations

$$\hat{x} = \frac{\sum_i \hat{x}_i w_i}{\sum_i w_i}$$

to obtain $x_i = \tilde{x}_i - \hat{x}$. We then define

$$t = \sum_i w_i$$

summing across the whole dataset. At each trial period we fold the light curve and accumulate into a set of bins j of width $W_{\rm b}'$ the following quantities

$$s_j = \sum_{i \in j} x_i w_i, \qquad r_j = \sum_{i \in j} w_i$$

The fitted transit depth in the bin, and its associated variance are then

$$\delta_j = \frac{s_j t}{r_j(t - r_j)}, \qquad \mathrm{Var}(\delta_j) = \frac{t}{r_j(t - r_j)}$$

and the signal-to-noise ratio of a putative transit in the bin is:

$$\mathcal{S}_j = \frac{\delta_j}{\sqrt{\mathrm{Var}(\delta_j)}} \qquad (5)$$
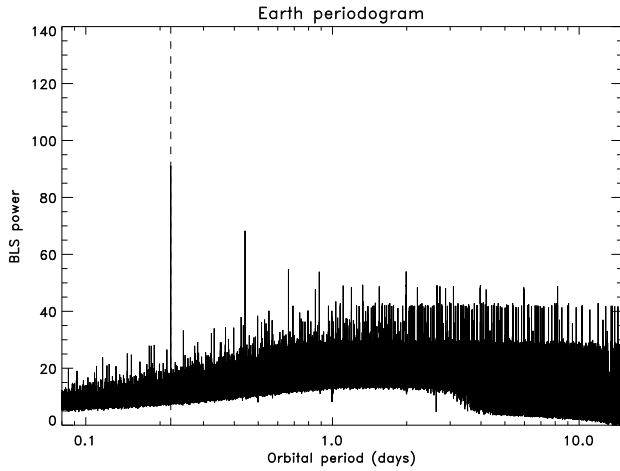
Figure 3. BLS power spectrum for the transit signal of an Earth-sized body in an orbit with a 5 hour period. While the correct (inserted) period is recovered (as indicated by the dashed line) by the standard implementation of the BLS algorithm, strong aliasing and noise structure are present, particularly at long periods.

For each epoch bin we compute the signal-to-noise $\mathcal{S}_{j,b}$ for each of our trial box widths by co-adding values of s_j and r_j in adjacent bins and find the maximum $\mathcal{S}_{j,max}$ over all of the box widths. The maximum value of $\mathcal{S}_{j,max}$ across all of the epoch bins then represents the significance of the detection of a transit at the given trial period. When computing this latter maximum we ignored trial boxes which contained less than five data points, or did not contain data points from at least five distinct orbits.

Figure 3 shows the periodogram computed in this fashion for the sample light curve shown in the lower panel of Figure 2, a $1.2\,\mathrm{R}_\oplus$ radius body in a 5 hour orbit. Although the correct simulated period shows up as the highest peak in the periodogram, there is significant non-random structure in the noise continuum, particularly for trial periods longer than 1 day. Our interpretation of this phenomenon is that it is a by-product of a few unique features of the transit signals we are dealing with. Firstly the duration of the transits, and hence the width of the boxes fitted by the BLS algorithm, is much shorter with respect to both the orbital period and the WASP survey cadence than for transits of main sequence stars. As a consequence the trial bins will contain many fewer data points than for a main sequence transit search, particularly at longer trial periods. Secondly as the transit signals are so deep compared to the main sequence case, they are less prone to being "washed out" when the light curve is folded on an incorrect trial period and the in-transit points spread across all orbital phases. In the case illustrated the Earth-sized body will cause transits with a depth of $\sim 70\%$. Even in a trial bin with, for example, 1 in-transit and 10 out-of-transit data points the presence of the single in-transit point would drag down the mean light level in the bin by more than 6%, which could be sufficient to be regarded as a significant detection.

To address this issue we modified equation 5 as follows

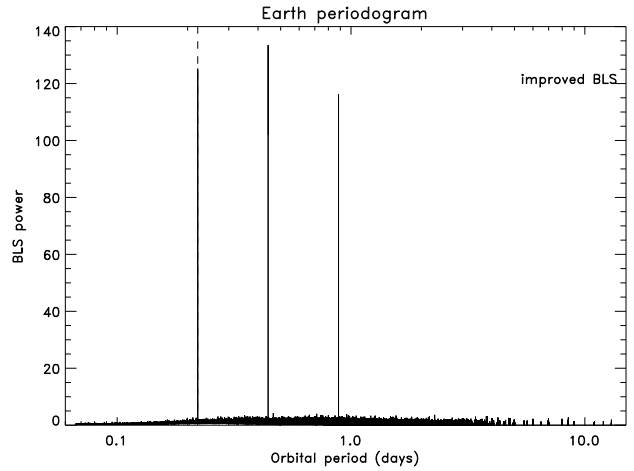$$\mathcal{S}'_j = \frac{\delta_j}{\sqrt{\mathrm{Var}(\delta_j) + \hat{d}_j^2}} \qquad (6)$$

Figure 4. BLS power spectrum as in Figure 3 obtained with the improved BLS routine. For the same transit signal we achieve higher S/N values and higher statistical significance for the detection. The strong aliasing and the noise structure seen in Figure 3 is much reduced.

where $\hat{d}_j^2$ is the mean-square deviation of the data points within the bin about their mean. This modification will have the effect of strongly reducing the computed signal-to-noise of bins which contain a mix of in-transit and out-of-transit data points. The magnitude of this down-weighting will tend to increase as the depth of the transit signal increases, but only in the cases in which the trial period does not match the true period (or an integer multiple or fraction). Where a bin contains just in-transit points the down-weighting will generally be small for all transit depths. Figure 4 shows the BLS periodogram computed using this modified prescription for the signal-to-noise, for the same transit as in Figure 3.

3.4 False detection rate

Automated searches for weak signals in noisy data are inherently susceptible to "false alarms", whereby a chance alignment of noise fluctuations in the data are misinterpreted by the search algorithm as a evidence likely detection of the signal being hunted. It is useful therefore to be able to define a filter which can be applied automatically to weed out these false detections. We achieved this by constructing synthetic light curves based on the time-sampling of sample WASP light curves which contain pure white-noise, but no simulated transit signal. We then computed BLS periodograms for these light curves in the same manner as for those containing simulated transits.

Kovács et al. (2002) define a useful metric for assessing the likely significance of a peak in a BLS periodogram, which they refer to as the Signal Detection Efficiency (SDE):

$$\mathrm{SDE} = \frac{\mathcal{S}_{\mathrm{peak}} - \bar{\mathcal{S}}}{\sigma_{\mathcal{S}}}$$

where $\mathcal{S}_{\mathrm{peak}}$ is the height of the peak, and $\bar{\mathcal{S}}$ and $\sigma_{\mathcal{S}}$ are measures of the mean level and scatter in the noise continuum of the periodogram. We computed the SDE of the highest peak in each of the synthetic, transitless light curves. The cumulative distribution function of these SDE measures over the whole sample is plotted in Figure 5. This
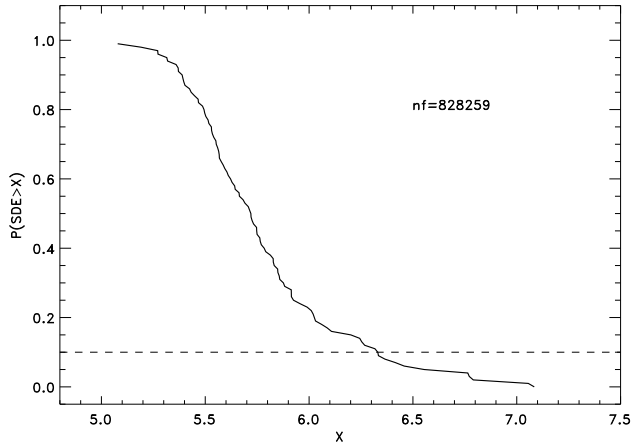
Figure 5. Probability Distribution Function (PDF) for the modified-optimised BLS routine. The dashed-line shows the detection threshold 6.3*SDE* for a 10% noise contribution.

distribution function allowed us to define a threshold SDE below which we could automatically discount a detection as likely to be a false alarm. As the size of the sample of WDs observed by WASP is fairly small, just a few hundred, we chose a relatively generous threshold ($SDE_{\mathrm{thresh}} = 6.3$) which would allow through around 10% of false detections. For larger surveys a more strict threshold might be necessary to avoid being swamped by false detections.

3.5 Recovery rates of synthetic transits

Figure 6 and Tables 1, 2 and 3 summarise our recovery rate for simulated transit signals injected into synthetic light curves of WDs of magnitudes V $\simeq$ 12, V $\simeq$ 13 and V $\simeq$ 15 respectively. We regard as a match any trial in which the most significant detected period is within 1% of being an integer fraction or multiple from $1/5\times$ to $5\times$ the injected transit signal.

We have attempted to separate out the various factors which can affect the efficiency of detection of these transit signals. When generating each synthetic light curve we can readily assess *a priori* whether it will fail the tests requiring a minimum number of individual transits and in-transit data points. We list in Tables 1, 2 and 3 the fraction f_{filt} which pass these two tests. It is evident from these tables that these requirements alone render transiting companions essentially undetectable at our longest trial periods (8.30 and 14.72 days) in a WASP-like survey; the transits are too short in duration and too infrequent to be adequately sampled. For companions around $1\,R_{\oplus}$ and larger however there is a good chance of detection out to periods of around 4 days, at least in principle.

The table also shows the impact of adding representative photometric noise on the detection rates (f_{det}). For the idealised photon-noise-limited case objects as small as Mercury could be detected to periods of around 1.5 d, and the Moon for periods less than 1 d. Once the impact correlated instrumental noise (red noise) is added, Moon-sized companions become almost undetectable, though the recovery
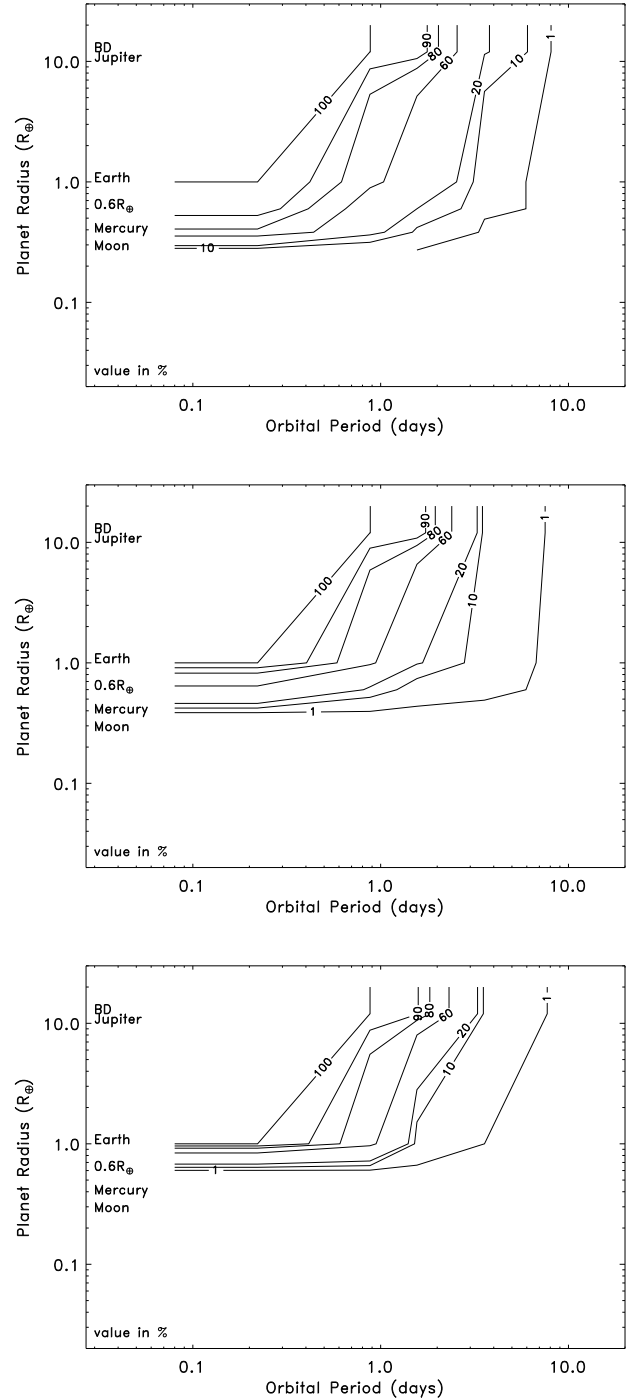
Figure 6. Recovery rate of simulated transits of a WD of magnitude V $\simeq$ 12 (top), V $\simeq$ 13 (middle) and V $\simeq$ 15 (bottom). The frequency contours are expressed in percentage values.

rates for larger bodies, particularly in short-period orbits, remains encouraging.

Our key conclusion from these simulations is that for the case of transits of WDs, the degree of photometric precision delivered by a survey is of somewhat secondary importance compared to a high cadence and continuous coverage. For planet-sized bodies individual transits will be quite deep and

Table 1. Recovery rate of simulated transits of a bright WD (V $\simeq$ 12). Results are shown for synthetic light curves containing white and red noise. In both cases f_{det} is the fraction of cases in which the highest peak in the periodogram satisfies our period matching criteria and has an SDE > 6.3, and f_{bt} is the fraction which match the period criteria but have SDE < 6.3. f_{filt} is the fraction of cases in which the synthetised light curves pass the requirements for a minimum number of transits (> 5) and data points (> 5) in transit. Dashes indicate cases in which the companion would be tidally disrupted within the WD's Roche radius.

Size	R_{pl} $R_{\oplus}$	δ_{tr} (%)	P (days)	D_{tr} (min)	f_{filt} (%)	White noise f_{det} (%)	f_{bt} (%)	red noise f_{det} (%)	f_{bt} (%)
BD-Gas Giant	10.0	100	0.08	5.65	100	100	0	100	0
			0.22	7.93	100	100	0	100	0
			0.87	12.55	100	100	0	100	0
			1.56	15.22	100	99	1	98	2
			3.57	20.05	69	24	25	21	32
			8.30	26.56	0.1	0	0	0	0
			14.72	32.15	0	0	0	0	0
Earth	1.0	49	0.08	−	−	−	−	−	−
			0.22	1.70	100	100	0	100	0
			0.87	2.65	96	76	5	67	10
			1.56	3.21	71	48	19	37	30
			3.57	4.23	14	5	7	2	4
			8.30	5.61	0	0	0	0	0
			14.72	6.82	0	0	0	0	0
0.6 $R_{\oplus}$	0.6	18	0.08	−	−	−	−	−	−
			0.22	1.42	100	98	2	96	4
			0.87	2.21	87	44	14	41	6
			1.56	2.68	51	31	17	20	19
			3.57	3.53	7	3	2	2	1
			8.30	4.67	0	0	0	0	0
			14.72	5.66	0	0	0	0	0
Mercury	0.34	5.7	0.08	−	−	−	−	−	−
			0.22	1.25	100	86	6	78	2
			0.87	1.98	78	25	26	24	19
			1.56	2.40	40	12	14	8	9
			3.57	3.17	4	2	0	0	0
			8.30	4.20	0	0	0	0	0
			14.72	5.10	0	0	0	0	0
Moon	0.27	3.6	0.08	−	−	−	−	−	−
			0.22	1.19	100	38	13	4	26
			0.87	1.87	74	12	24	1	30
			1.56	2.27	35	4	33	1	37
			3.57	2.99	3	0	0	0	0
			8.30	3.96	0	0	0	0	0
			14.72	4.79	0	0	0	0	0

readily detectable in data of moderate photometric quality, however it is the short duration of the transits that is the main factor limiting the transit detection rate in surveys optimised for main sequence stars.

4 SEARCHING FOR TRANSIT SIGNALS IN WASP SURVEY DATA

Encouraged by the results of our simulations we selected a sample of WDs, which have been routinely monitored by WASP through the 2004–2008 observing seasons, and performed a systematic search for eclipsing and transiting substellar and planetary companions. We selected the sample by cross-correlating the catalogue of WASP objects for which more than 600 data points are available with the McCook & Sion catalogue (McCook & Sion 2003). The resulting sample of 194 WDs with magnitude V < 15 is presented in Table 4.

We searched the sample for transits and eclipses using our implementation of the BLS algorithm, searching periods ranging from 2 hours to 15 days. In addition we have also inspected each of the individual light curves by eye. In

both searches we found no evidence for any transiting and eclipsing companions within the period range searched in this study. We have used this null result together with the results of our simulations to estimate an upper-limit to the frequency of such close companions for the sample of WDs considered in this study.

4.1 Limits on frequency of companions to WDs

In order to estimate an upper limit to the frequency of close substellar and planetary companions to WDs, we used the detection limits derived from our simulations and the results obtained from the analysis of the sample of 194 WDs. We first used a binomial distribution to describe the probability $\mathcal{P}(n; N, f)$ of finding n transiting companions for a given sample of N stars, with a true companion frequency f (e.g.. see McCarthy & Zuckerman 2004; and Appendix of Burgasser et al. 2003) as follows:

$$\mathcal{P}(n; N, f) = \frac{N!}{n!(N-n)!} f^n (1-f)^{N-n} \qquad (7)$$

When the two quantities N and n are known equation 7 can be used to derive the distribution ($\mathcal{P}_1$) describing the probability of f, where f is the frequency of transiting companions. The probability $\mathcal{P}_1(f; n, N)$ is proportional to $\mathcal{P}(n; N, f)$ for f in the interval $[0, 1]$. We obtain $\mathcal{P}_1$ by normalising :

$$\int_0^1 \mathcal{P}_1(f; n, N) \, df \ = 1 \qquad (8)$$

which yields $\mathcal{P}_1 = (N+1)\mathcal{P}$.

   Although our complete sample numbers $N = 194$ stars, we have already established that even if all of these have companions only a fraction $p_{tr}(R_p, P)$ will exhibit a transit, and of those which do exhibit a transit only a fraction $p_{det}(R_p, P)$ would be detectable in a WASP-like survey. Both of these factors will act to reduce the total number of transiting companions detected in the survey, or in the case of a null result will tend to weaken the constraints that can be placed on true companion frequency by such a survey. To incorporate these factors we modified our effective sample size as:

$$N' = N \times p_{tr}(R_p, P) \times p_{det}(R_p, P)$$

   and used this in Eq. 8, which we integrated to find the limiting companion frequency f_{lim} that encloses 95% of the probability distribution. Figure 7 (top panel) shows the upper-limit on companion frequency for a null detection in a "perfect" survey in which $p_{det} = 1$ and a sample size $N = 194$. In such a survey the detectability of companions is limited solely by the intrinsic probability of them transiting their host.

   To factor in the efficiency of detection of transits in a WASP-like survey we need to determine a representative $p_{det}(R_p, P)$. Our simulations were performed at only three specific host-star magnitudes, whereas the distribution of the magnitudes of the stars in our sample is of course a continuum (covering the range V $\sim 9 - 15$). We therefore combine the three magnitude-specific p_{det} maps (Figure 6) into a single map by interpolating/extrapolating according
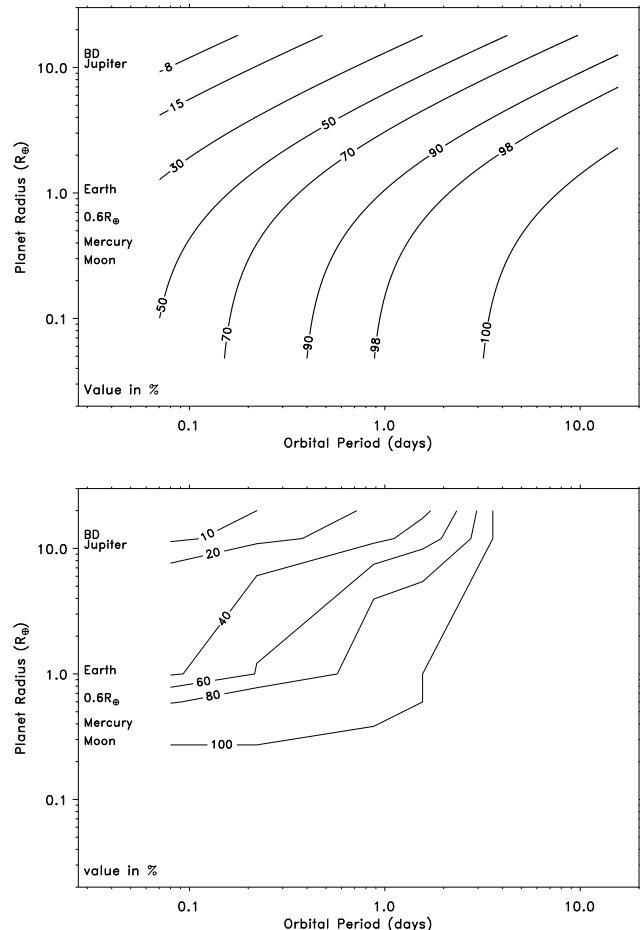
Figure 7. Top panel: upper-limit on companion frequency inferred from a null detection in a survey sample of size $N = 194$ assuming perfect detectability of transits across the parameter space. Lower panel: limits in the same sample folding in the detectability of transiting systems in a WASP-like survey. In both panels the frequency contours are expressed in percentage values.

to the magnitude of each object in our sample and combining these to form an averaged map which can be folded in to our calculation of the upper-limits. The resulting limits corresponding to the 95% of the integrated probability, are shown in in the lower panel of Figure 7. Our results show that for rocky bodies smaller than the size of Mercury no useful upper limits to the frequency of companions to WDs can be found, and that for Earth-sized companions only weak constraints can be imposed. However, it does suggest that objects the size of brown dwarfs or gas giants with orbital periods P< $0.1 - 0.2$ days must be relatively rare (upper limit of $\sim 10\%$).

5 CONCLUSION

We have used a modified version of the Box Least Squares algorithm to investigate the detection limits for substellar and planetary companions to WDs achievable using data already available in the WASP photometric survey. Our simulations proved extremely encouraging, suggesting that plan-

etary bodies as small as Mercury at small orbital radii can be detected with good photometric data even in the presence of red noise. For smaller bodies red noise in the light curves becomes increasingly problematic, while for bodies with larger orbital periods, the absence of significant numbers of in-transit points, significantly decreases the detection sensitivity.

Application of our modified BLS algorithm to search for companions to WDs in a sample of 194 stars in the magnitude range V $\sim$ 9–15, available in the WASP archive, did not reveal any eclipsing or transiting substellar or planetary companions. Visual inspection of individual light curves for the WDs in our sample confirmed the absence of significant periodic dropouts in the WASP data. We have used the non-detection of planetary companions to the WDs in our sample together with the estimated detection sensitivities determined from our simulations, to place upper limits to the frequency of substellar and planetary companions to white dwarfs. While no useful limits can be placed on the likely frequency of Mercury-sized or smaller companions, and only weak constraints on the frequency of Earth-sized objects in the closest orbits, slightly stronger constraints can be placed on the frequency of larger bodies in very short-period orbits. For example, brown dwarfs and gas giants radius $\approx$ R$_{jup}$ with periods $< 0.1-0.2$ days, similar to the known WD+BD binary WD0137 $-$ 349 (Maxted et al. 2006), must certainly be relatively rare ($\lesssim 10\%$). Of course, this limit needs to be compared with those derived from other sources, e.g. infrared sky surveys. For example, Farihi et al. (2005) estimated that $< 0.5\%$ of WDs have L dwarf companions, while Steele et al. (in prep.) tentatively suggests the fraction of unresolved brown dwarf companions (including T dwarfs) may be slightly higher, between $1 - 2\%$. From Spitzer photometry Farihi et al. (2008) suggests that $< 4\%$ of white dwarfs have unresolved substellar companions $> 10\,M_{jup}$, although the limits at lower masses (e.g. $< 6\,M_{jup}$) are considerably weak.

To place more stringent constraints on close substellar and gas giant companions to WDs, and similarly stringent constraints on Earth size bodies in close orbital separations likely requires significantly larger WD samples. In addition, our simulations and analysis of WD light curves in the WASP archive suggests the degree of photometric precision is of somewhat secondary importance compared to a high cadence and continuous coverage. The short duration of eclipses and transits of WDs ($\approx 5 - 20$ mins for companions radius $\approx$ R$_{jup}$; $\approx 1 - 5$ mins for terrestrial bodies) compared to the ≈ 8 min cadence of WASP observations, appears to be the main factor limiting the transit detection rate in a survey optimised for planetary transits of main sequence stars.

Future surveys such as Pan-STARRS and LSST will be capable of detecting tens of thousands of WDs. However, we emphasise that observations of high cadence and long baseline are of greatest benefit when attempting to detect the signature of close, eclipsing and transiting substellar and planetary companions to WDs. Space missions such as *COROT*, *Kepler* (see Di Stefano et al. 2010) and, especially, *PLATO* may therefore be better suited to a survey of WDs as they deliver uninterrupted coverage at high cadence and exquisite photometric precision ($\sim 10^{-4} - 10^{-5}$) and could

at least in principle detect the transits of asteroid-sized bodies across a WD.

6 ACKNOWLEDGMENTS

Table 2. Recovery rate of simulated transits of a V $\simeq$ 13 WD

Size	$R_{\rm pl}$ $R_{\oplus}$	$\delta_{\rm tr}$ (%)	P (days)	$D_{\rm tr}$ (min)	$f_{\rm filt}$ (%)	White noise $f_{\rm det}$ (%)	$f_{\rm bt}$ (%)	red noise $f_{\rm det}$ (%)	$f_{\rm bt}$ (%)
BD-Gas Giant	10.0	100	0.08	5.65	100	100	0	100	0
			0.22	7.93	100	100	0	100	0
			0.87	12.55	100	100	0	100	0
			1.56	15.22	100	95	2	98	0
			3.57	20.05	69	24	25	6	31
			8.30	26.56	0.1	0	5	0	7
			14.72	32.15	0	0	0	0	1
Earth	1.0	49	0.08	—	—	—	—	—	—
			0.22	1.70	100	100	0	100	0
			0.87	2.65	96	74	11	64	6
			1.56	3.21	71	37	30	21	17
			3.57	4.23	14	2	34	3	36
			8.30	5.61	0	0	4	0	5
			14.72	6.82	0	0	0	0	2
$0.6\,{\rm R}_{\oplus}$	0.6	18	0.08	—	—	—	—	—	—
			0.22	1.42	100	84	1	55	29
			0.87	2.21	87	42	11	16	26
			1.56	2.68	51	15	20	4	53
			3.57	3.53	7	3	35	2	37
			8.30	4.67	0	0	5	0	4
			14.72	5.66	0	0	2	0	0
Mercury	0.45	10	0.08	—	—	—	—	—	—
			0.22	1.25	100	22	19	0	8
			0.87	1.98	78	16	15	0	26
			1.56	2.40	40	13	22	0	51
			3.57	3.17	4	1	35	0	35
			8.30	4.20	0	0	4	0	4
			14.72	5.10	0	0	2	0	0
Moon	0.27	3.6	0.08	—	—	—	—	—	—
			0.22	1.19	100	12	8	0	8
			0.87	1.87	74	8	15	0	26
			1.56	2.27	35	3	23	0	50
			3.57	2.99	3	0	35	0	35
			8.30	3.96	0	0	4	0	4
			14.72	4.79	0	0	2	0	0

Table 3. Recovery rate of simulated transits of a V $\simeq$ 15 WD

Size	$R_{\rm pl}$ R$_\oplus$	$\delta_{\rm tr}$ (%)	P (days)	$D_{\rm tr}$ (min)	$f_{\rm filt}$ (%)	White noise $f_{\rm det}$ (%)	$f_{\rm bt}$ (%)	red noise $f_{\rm det}$ (%)	$f_{\rm bt}$ (%)
BD-Gas Giant	10.0	100	0.08	5.65	100	100	0	100	0
			0.22	7.93	100	100	0	100	0
			0.87	12.55	100	100	0	100	0
			1.56	15.22	100	98	0	91	3
			3.57	20.05	69	4	33	8	44
			8.30	26.56	0.1	0	5	0	8
			14.72	32.15	0	0	0	0	2
Earth	1.0	49	0.08	—	—	—	—	—	—
			0.22	1.70	100	100	0	100	0
			0.87	2.65	96	65	11	66	8
			1.56	3.21	71	37	30	6	43
			3.57	4.23	14	2	34	1	49
			8.30	5.61	0	0	4	0	7
			14.72	6.82	0	0	0	0	1
0.6 R$_\oplus$	0.6	18	0.08	—	—	—	—	—	—
			0.22	1.42	100	10	18	0	9
			0.87	2.21	87	7	17	0	27
			1.56	2.68	51	4	44	0	52
			3.57	3.53	7	1	50	0	36
			8.30	4.67	0	0	7	0	4
			14.72	5.66	0	0	1	0	0
Mercury	0.45	10	0.08	—	—	—	—	—	—
			0.22	1.25	100	5	8	0	8
			0.87	1.98	78	5	18	0	26
			1.56	2.40	40	3	45	0	50
			3.57	3.17	4	0	49	0	35
			8.30	4.20	0	0	6	0	4
			14.72	5.10	0	0	1	0	0
Moon	0.27	3.6	0.08	—	—	—	—	—	—
			0.22	1.19	100	4	7	0	8
			0.87	1.87	74	4	18	0	26
			1.56	2.27	35	1	43	0	49
			3.57	2.99	3	0	49	0	35
			8.30	3.96	0	0	6	0	4
			14.72	4.79	0	0	0	0	0

1SWASP	WD	V (WASP)	N
J000007.24+295700.6	2357+296	12.24	15825
J000331.62−164358.4	0000−170	14.87	10446
J000732.24+331727.7	0004+330	13.95	21067
J000818.17+512316.7	0005+511	13.42	4876
J002130.72−262611.0	0018−267	13.92	7305
J003112.96−271253.7	0028−274	14.99	6961
J003145.95+571817.1	0029+571	10.50	2511
J003353.90−270823.6	0031−274	14.30	7293
J003952.15+313229.3	0037+312	15.03	9429
J004121.46+555009.1	0038+555	13.47	6202
J005317.46−325956.6	0050−332	13.45	9316
J005340.53+360118.4	0050+357	14.54	14264
J011011.78+270104.8	0107+267	15.61	4702
J011018.59−340025.5	0107−342	14.27	10151
J011211.65−261327.7	0109−264	13.14	10038
J011547.45−240651.0	0113−243	15.03	29846
J012942.57+422817.1	0126+422	13.51	18136
J013856.85+152742.5	0136+152	14.37	2251
J014754.80+233943.8	0145+234	14.19	4653
J015202.95+470005.5	0148+467	12.08	4362
J020253.98−165303.5	0200−171	11.41	8756
J021255.35+170356.5	0210+168	14.32	3082
J021616.34+395125.5	0213+396	14.11	7608
J021733.49+570647.3	0214+568	13.29	2279
J022440.83+400823.0	0221+399	10.02	13621
J023530.74+571524.8	0231+570	13.68	2223
J023619.55+524412.4	0232+525	13.76	6096
J024502.37−171220.5	0242−174	15.54	7672
J031149.19+190055.7	0308+188	14.46	2711
J031315.18+190824.5	0310+188	16.20	2547
J031445.95+481206.1	0311+480	14.33	4908
J031942.73+344223.8	0316+345	14.37	7868
J034329.01−454904.2	0341−459	15.19	15506
J035024.96+171447.4	0347+171	9.47	2515
J035630.59−364119.7	0354−368	12.66	9400
J035705.82+283751.5	0353+284	11.67	5606
J040434.12+250851.8	0401+250	13.58	3841
J041010.32+180223.8	0407+179	14.50	2303
J044321.26+464205.7	0441+467	12.76	4283
J045013.52+174206.1	0447+176	12.09	3155
J045535.93−292900.0	0453−295	15.58	9872
J045713.22−280752.8	0455−282	13.90	9869
J045722.55+415556.6	0453+418	11.98	5475
J050003.17−362346.4	0458−364	13.33	13986
J050355.38−285436.0	0501−289	13.58	8629
J050530.60+524951.9	0501+527	11.72	3288
J051233.54+165209.6	0509+168	13.47	2931
J051302.56+162246.8	0510+163	14.15	2930
J052906.46+271257.6	0526+271	15.17	9014
J053244.82+261200.7	0529+261	14.14	7321
J053620.20+412955.7	0532+414	13.46	5935

1SWASP	WD	V (WASP)	N
J054748.47+280311.6	0544+280	13.04	5246
J055814.64−373426.1	0556−375	14.64	10756
J061000.36+281428.4	0606+282	13.00	3538
J061518.70+174341.9	0612+177	13.37	2676
J061934.22+553642.9	0615+556	13.40	3258
J062312.60−374127.9	0621−376	12.09	11875
J062702.01−252249.7	0625−253	12.98	9502
J064112.82+474419.8	0637+477	14.52	2673
J064856.08−252347.0	0646−253	13.74	9658
J071736.26+582420.4	0713+584	12.03	2993
J073427.45+484115.6	0730+487	14.96	5327
J082705.14+284402.6	0824+288	14.27	9142
J084253.04+230025.6	0839+231	14.45	3552
J084644.40+353833.7	0843+358	14.72	7568
J084909.48+342947.8	0846+346	15.47	6769
J085730.45+401613.2	0854+404	15.16	11310
J090148.65+360708.1	0858+363	14.87	9274
J092921.28−041005.9	0926−039	14.57	1030
J094159.32+065717.1	0939+071	15.11	1621
J094250.60+260100.1	0939+262	14.88	4173
J094846.64+242126.0	0945+245	14.47	4244
J101628.64−052032.8	1013−050	13.21	1362
J101801.63+072123.9	1015+076	15.59	1179
J102405.90+262103.7	1021+266	9.33	7073
J102459.84+044610.5	1022+050	14.16	3186
J102712.01+322329.8	1024+326	13.51	9985
J102909.80+020553.7	1026+023	14.05	2885
J103936.73+430609.2	1036+433	11.17	4800
J104616.19−034033.4	1043−034	14.14	1913
J105220.53−160804.3	1049−158	14.59	7601
J105443.32+270657.2	1052+273	13.73	4875
J105709.94+301336.8	1054+305	14.69	5270
J110432.58+361049.1	1101+364	14.87	5109
J111912.41+022033.1	1116+026	14.82	2222
J111934.60−023903.1	1117−023	14.61	3512
J112542.87+422358.3	1122+426	13.25	6053
J112619.09+183917.2	1123+189	14.20	4600
J112910.93+380850.1	1126+384	15.22	9645
J112918.04+181645.8	1126+185	14.10	2932
J113227.35+151731.0	1129+155	14.26	2853
J113423.42+314605.9	1131+320	14.94	10834
J113705.10+294758.1	1134+300	12.64	9241
J114359.35+072906.1	1141+077	14.47	2810
J114803.16+183046.6	1145+187	14.38	7930
J115006.09−231613.8	1148−230	14.56	14440
J115119.30+125359.8	1148+131	14.15	3680
J115154.20+052839.7	1149+057	15.37	5172
J120145.98−034540.6	1159−034	15.04	2630
J120526.70−233312.3	1202−232	12.90	14521
J120936.01−033307.6	1207−032	13.69	2636
J121229.13−062206.8	1209−060	13.39	2608
J121233.90+134625.0	1210+140	14.78	3027
J121356.28+325631.6	1211+332	14.93	11489

1SWASP	WD	V (WASP)	N
J121410.52−171420.2	1211−169	10.15	19365
J122747.36−081438.0	1225−079	16.06	1347
J123515.36+233419.4	1232+238	13.63	8160
J124428.57−011858.1	1241−010	13.51	3307
J125217.16+154444.2	1249+160	15.00	10250
J125223.56+175651.6	1249+182	15.43	10340
J125514.83+373229.3	1253+378	15.58	8160
J125702.33+220152.9	1254+223	13.67	18254
J131341.59−305133.5	1310−305	14.92	14136
J131621.95+290556.3	1314+293	12.77	8381
J132115.12+462324.0	1319+466	14.97	8291
J133601.94+482846.7	1333+487	13.89	8310
J133741.51+363903.8	1335+369	14.51	9836
J133913.55+120831.0	1336+123	14.89	3770
J134117.94+342153.6	1339+346	14.93	8492
J134307.26−310151.4	1340−307	13.25	11366
J135153.93+140945.6	1349+144	14.77	3288
J141026.96+320836.1	1408+323	14.22	7984
J141329.93+213730.0	1411+218	13.86	5943
J142439.16+091714.2	1422+095	14.90	2935
J143545.65−163818.1	1432−164	14.58	13190
J144814.07+282511.6	1446+286	14.71	16402
J145156.24+422142.9	1450+425	15.57	8167
J151127.61+320417.9	1509+322	13.10	3865
J151714.27+031028.0	1514+033	13.79	4115
J152950.39+085546.3	1527+090	14.72	3552
J154419.46+180643.9	1542+182	15.08	4373
J155501.99+351328.6	1553+353	14.74	12136
J155804.76−090807.3	1555−089	13.37	3793
J160521.18+430436.6	1603+432	15.32	1353
J160532.09+122542.8	1603+125	15.91	3148
J161053.25+114353.6	1608+118	14.61	3466
J161419.14−083326.4	1611−084	13.43	3792
J161623.83+265310.7	1614+270	14.82	14663
J161928.99−390711.5	1616−390	14.63	11944
J162333.83−391346.1	1620−391	11.09	12748
J163339.30+393053.6	1631+396	13.88	31052
J164539.13+141746.3	1643+143	15.69	3436
J164718.40+322833.0	1645+325	13.90	27543
J170033.62+441024.3	1659+442	13.27	43025
J170530.69+480311.4	1704+481	13.93	20729
J172643.19+583732.0	1725+586	13.44	10838
J175255.81+094751.9	1750+098	9.53	1425
J175332.27+103724.3	1751+106	14.15	4268
J181140.81+282939.5	1809+284	14.06	5172
J182029.78+580441.2	1819+580	14.23	3511
J182337.00+410402.2	1822+410	14.63	18410
J191858.65+384321.8	1917+386	11.58	1700
J194740.52−420026.3	1944−421	10.30	23397
J195219.66−384613.8	1948−389	13.34	32011
J200039.25+014341.9	1958+015	12.48	2948
J202706.23+553415.0	2025+554	12.98	6313
J202956.18+391332.3	2028+390	12.45	2902

continued from previous page

1SWASP	WD	V (WASP)	N
J203202.39+183139.6	2029+183	12.20	12648
J203454.59−273449.2	2031−277	15.28	6762
J203838.16−332635.0	2035−336	14.25	12714
J204808.16+395137.8	2046+396	14.94	2942
J204906.71+372813.2	2047+372	12.74	2989
J210031.30+505118.0	2058+506	15.93	3907
J211244.06+500618.1	2111+498	12.93	3354
J211652.86+241214.9	2114+239	12.39	4421
J211708.29+341227.6	2115+339	12.33	2117
J211717.80+504407.3	2115+505	11.55	3392
J211856.30+541241.4	2117+539	11.99	6914
J212146.78−331048.0	2118−333	14.27	7625
J212454.89+155903.8	2122+157	13.80	12929
J212458.14+282603.5	2122+282	14.60	2969
J212743.10−221148.4	2124−224	14.94	11028
J213636.12+220433.5	2134+218	14.53	13813
J213652.94+124719.5	2134+125	13.35	11732
J213846.20+230917.6	2136+229	12.28	14626
J214954.57+281659.8	2147+280	15.04	16920
J215202.73+372617.9	2149+372	12.59	9941
J215453.40−302918.4	2151−307	15.05	7776
J215618.25+410245.5	2154+408	14.61	3191
J220714.40+072232.3	2204+071	14.91	7675
J221029.22−300543.7	2207−303	13.61	11058
J222919.42−444138.4	2226−449	14.48	10279
J223822.75+313418.4	2236+313	14.75	11464
J225848.13+251544.0	2256+249	12.63	13430
J230740.13−342753.4	2304−347	14.86	10752
J231219.65+260419.7	2309+258	14.57	9279
J232606.58+160019.4	2323+157	13.63	4815
J232715.83+400124.7	2324+397	15.41	21231
J233135.65+410130.6	2329+407	14.18	17476
J233149.93−285252.6	2329−291	14.29	10859
J233536.58−161743.8	2333−165	13.57	5660
J234350.87+323247.2	2341+322	13.28	11404
J235530.18−251612.7	2352−255	13.61	10780
J235644.76−301631.6	2354−305	15.01	10635

WDs observed by WASP, including the WASP identity, corresponding identity in the McCook & Sion catalogue, WASP magnitude, and the number of individual data points contributing to the light curve in the WASP archive. The WASP magnitude is defined as $-2.5\log_{10}(F/10^6)$, where F is the mean WASP flux in μVega; it is a pseudo-V magnitude comparable to the Tycho-V magnitude.

REFERENCES

Alonso R., Brown T. M., Torres G., Latham D. W., Sozzetti A., Mandushev G., Belmonte J. A., Charbonneau D., Deeg H. J., Dunham E. W., O'Donovan F. T., Stefanik R. P., 2004, ApJ, 613, L153

Bakos G., Noyes R. W., Kovács G., Stanek K. Z., Sasselov D. D., Domsa I., 2004, PASP, 116, 266

Bakos G. Á., et al., 2010, ApJ, 710, 1724

Becklin E. E., Zuckerman B., 1988, Nature, 336, 656

Brown T. M., Charbonneau D., 2000, in Garzón G., Eiroa C., de Winter D., Mahoney T. J., eds, Disks, Planetesimals, and Planets Vol. 219 of Astronomical Society of the Pacific Conference Series, The STARE Project: a Transit Search for Hot Jupiters. pp 584–+

Burgasser A. J., Kirkpatrick J. D., Reid I. N., Brown M. E., Miskey C. L., Gizis J. E., 2003, ApJ, 586, 512

Burleigh M. R., Clarke F. J., Hodgkin S. T., 2002, MNRAS, 331, L41

Burleigh M. R., Hogan E., Dobbie P. D., Napiwotzki R., Maxted P. F. L., 2006, MNRAS, 373, L55

Collier Cameron A., et al., 2006, MNRAS, 373, 799

Day-Jones A. C., et al., 2010, MNRAS, pp 1639–+

Debes J. H., Sigurdsson S., 2002, ApJ, 572, 556

Di Stefano R., Howell S. B., Kawaler S. D., 2010, ApJ, 712, 142

Dobbie P. D., Burleigh M. R., Levan A. J., Barstow M. A., Napiwotzki R., Holberg J. B., Hubeny I., Howell S. B., 2005, MNRAS, 357, 1049

Duncan M. J., Lissauer J. J., 1998, Icarus, 134, 303

Dunham E. W., Mandushev G. I., Taylor B. W., Oetiker B., 2004, PASP, 116, 1072

Farihi J., Becklin E. E., Zuckerman B., 2005, ApJ, 161, 394

Farihi J., Becklin E. E., Zuckerman B., 2008, ApJ, 681, 1470

Farihi J., Christopher M., 2004, AJ, 128, 1868

Farihi J., Jura M., Zuckerman B., 2009, ApJ, 694, 805

Farihi J., Zuckerman B., Becklin E. E., 2008, ApJ, 674, 431

Frink S., Mitchell D. S., Quirrenbach A., Fischer D. A., Marcy G. W., Butler R. P., 2002, ApJ, 576, 478

Hansen B. M. S., 2002, in M. M. Shara ed., Stellar Collisions, Mergers and their Consequences Vol. 263 of Astronomical Society of the Pacific Conference Series, Stellar Collisions and Pulsar Planets. pp 221–+

Hatzes A. P., Guenther E. W., Endl M., Cochran W. D., Döllinger M. P., Bedalov A., 2005, A&A, 437, 743

Hogan E., Burleigh M. R., Clarke F. J., 2009, MNRAS, 396, 2074

Jeans J. H., 1924, MNRAS, 85, 2

Jura M., 2003, ApJ, 584, L91

Jura M., Farihi J., Zuckerman B., 2009, AJ, 137, 3191

King A. R., 1988, QJRAS, 29, 1

Kovács G., Zucker S., Mazeh T., 2002, A&A, 391, 369

Littlefair S. P., Dhillon V. S., Marsh T. R., Gänsicke B. T., Baraffe I., Watson C. A., 2007, MNRAS, 381, 827

Littlefair S. P., Dhillon V. S., Marsh T. R., Gänsicke B. T., Southworth J., Watson C. A., 2006, Science, 314, 1578

Littlefair S. P., Dhillon V. S., Martín E. L., 2003, MNRAS, 340, 264

Livio M., Pringle J. E., Wood K., 2005, ApJ, 632, L37

Maxted P. F. L., Napiwotzki R., Dobbie P. D., Burleigh M. R., 2006, Nature, 442, 543

Mayor M., Queloz D., 1995, Nature, 378, 355

McCarthy C., Zuckerman B., 2004, AJ, 127, 2871

McCook G. P., Sion E. M., 2003, VizieR Online Data Catalog, 3235, 0

McCullough P. R., Stys J. E., Valenti J. A., Fleming S. W., Janes K. A., Heasley J. N., 2005, PASP, 117, 783

Mullally F., Winget D. E., Degennaro S., Jeffery E., Thompson S. E., Chandler D., Kepler S. O., 2008, ApJ, 676, 573

Parsons S. G., Marsh T. R., Copperwheat C. M., Dhillon V. S., Littlefair S. P., Gänsicke B. T., Hickman R., 2010, MNRAS, 402, 2591

Parthasarathy M., Branch D., Jeffery D. J., Baron E., 2007, New Astronomy Review, 51, 524

Patterson J., 1998, PASP, 110, 1132

Patterson J., Thorstensen J. R., Kemp J., 2005, PASP, 117, 427

Pollacco D. L., et al., 2006, PASP, 118, 1407

Rasio F. A., Tout C. A., Lubow S. H., Livio M., 1996, ApJ, 470, 1187

Reach W. T., Kuchner M. J., von Hippel T., Burrows A., Mullally F., Kilic M., Winget D. E., 2005, ApJ, 635, L161

Sackett P. D., 1999, in Mariotti J.-M., Alloin D., eds, NATO ASIC Proc. 532: Planets Outside the Solar System: Theory and Observations Searching for Unseen Planets via Occultation and Microlensing. pp 189–+

Samus N. N., Durlevich O. V., et al. 2004, VizieR Online Data Catalog, 2250, 0

Sato B., et al., 2003, ApJ, 597, L157

Silvotti R., et al., 2007, Nature, 449, 189

Steele P. R., Burleigh M. R., Farihi J., Gänsicke B. T., Jameson R. F., Dobbie P. D., Barstow M. A., 2009, A&A, 500, 1207

Udalski A., Paczynski B., Zebrun K., Szymanski M., Kubiak M., Soszynski I., Szewczyk O., Wyrzykowski L., Pietrzynski G., 2002, Acta Astronomica, 52, 1

Villaver E., Livio M., 2007, ApJ, 661, 1192

Wickramasinghe D. T., Farihi J., Tout C. A., Ferrario L., Stancliffe R. J., 2010, MNRAS, 404, 1984